Diffraction of virtual and real photons

V.I. Alekseev,[a] **A.N. Eliseyev,**[a] **E. Irribarra,**[b,1] **I.A. Kishin,**[a,c] **A.S. Klyuev,**[a,c] **A.S. Kubankin,**[a,c] **R.M. Nazhmudinov**[a,c] **and S.V. Trofymenko**[d,e]

[a]*P.N. Lebedev Physical Institute RAS,*
53, Leninskiy Prospekt, 308007, Moscow, Russia

[b]*Escuela Politécnica Nacional, Departamento de Física,*
Ladrón de Guevara E11-253, Quito, Ecuador

[c]*Belgorod National Research University,*
85, Pobedy St., Belgorod, 308015, Russia

[d]*Akhiezer Institute for Theoretical Physics of National Science Center "Kharkov Institute of Physics and Technology",*
Akademicheskaya st., 1, Kharkov 61108, Ukraine

[e]*Karazin Kharkiv National University,*
4 Svobody sq., 61022 Kharkiv, Ukraine

E-mail: esteban.irribarra@epn.edu.ec

ABSTRACT: Parametric X-ray radiation associated with the diffraction of virtual photons and the diffraction of X-rays described as the diffraction of real photons are studied experimentally. The diffracted radiation was generated by a 7 MeV beam of electrons and an X-ray tube respectively. Both diffraction mechanisms occur in a tungsten powder. The processes have been compared excluding three key parameters: the attenuation in the target, the background of the diffracted signal and the spectrum of the incident radiation. Remarkable differences between the diffraction mechanisms of virtual and real photons are observed. The ratio between the PXR peak and the XRD peak decreases when the peak energy increases.

KEYWORDS: X-ray generators and sources; X-ray diffraction detectors; X-ray monochromators; Radiation damage evaluation methods

---

[1]Corresponding author.

Contents

1 Introduction

Parametric X-ray radiation (PXR) occurs when a charged particle interacts with atoms of an ordered structure such crystals. The Coulomb field of the incident particles excites the electrons of the target which radiate coherently due to the structure. The mechanism of radiation has a quasi Cherenkov nature [1–4].

At ultrarelativistic velocities of a charged particle its Coulomb field considerably shrinks in the direction of the particle motion and stretches in the orthogonal one, resembling a flat 'pancake'. In this case both the electric and magnetic fields created by the particle are almost perpendicular to its velocity and the whole proper field of the particle, moving almost with the speed of light, strongly resembles a plane electromagnetic wave with a very broad frequency spectrum. Due to this fact, many processes of the particle interaction with matter, involving the ionization loss and various types of radiation emission, can be treated with the use of the Weizsacker-Williams method of virtual photons [5, 6] (the idea of this method was initially proposed by E. Fermi [7]). In this method the Coulomb field of the incident particle is considered as a flux of quasi-real (or virtual) photons and the processes, taking place upon the particle motion in substance, are associated with the scattering and absorption of these photons (treated as real ones) by the atoms. Particularly, in this method the process of PXR can be treated as the Bragg diffraction of the virtual photons on the crystalline structure [8].

The spectral and angular characteristics of PXR are determined by both the incident beam of charged particles (Lorentz factor, divergence) and the parameters of the target (grain size and atom structure quality and the unit cell parameter). It should be mentioned that the spectral and angular characteristics of diffracted broadband X-rays (XRD) are similar to those of PXR if the angular distribution of the incident X-ray beam is close to the angular distribution of the virtual photons of the charged particle Coulomb field.

During a real process in which relativistic charged particles interact with matter, several radiation mechanisms play an important role giving a contribution to the total radiation yield. This feature complicates the separation between the contributions of virtual and real photons to the total radiation. This issue was widely analysed in [9] where a method to separate the contributions of

virtual and real photons to the total radiation yield was proposed based on the velocities difference of the charged particles (virtual photons) and free X-rays.

This work study more deeply the differences in the diffraction processes of virtual and real photons.

2   Experimental setup

The experiments were performed in the Department of High Energy Physics of the Lebedev Physical Institute of the RAS. In figure 1 is shown the scheme of the experiments. To guarantee an identical geometry for the diffraction of both virtual and real photons, the sources were installed in the same flange.
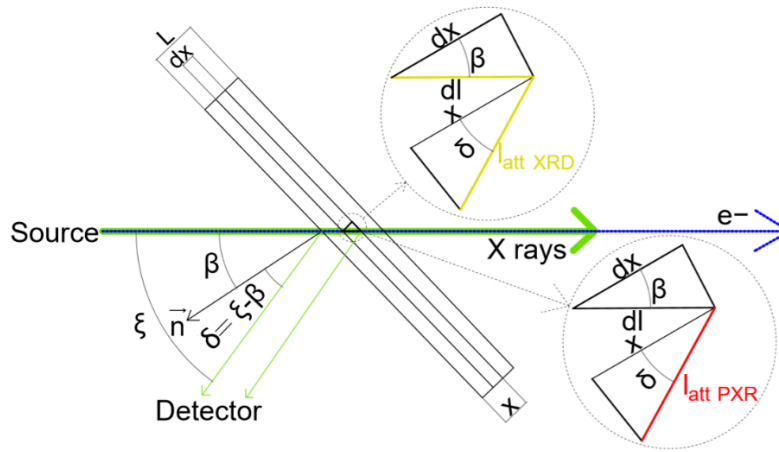
Figure 1. Experimental scheme. The source indicates the place where were installed the vacuum channel from the microtron in the first experiment and the X-ray tube in the second experiment. The path the photons travel inside the target in the case of both XRD and PXR is illustrated by $l_{att\ XRD}$ and $l_{att\ PXR}$. θ — observation angle, $\xi = \pi - \theta$, β — angle between the direction of propagation of the incident radiation and the target normal.

The source of the incident radiation for the diffraction study of virtual photons was a 7 MeV electron beam produced by a microtron. In order to increase the number of grains that takes part in the radiation process the magnetooptical system was adjusted for the beam of electrons to have a considerable large diameter 10 mm with an initial divergence smaller than 15 mrad at the target position. The beam position and current were monitored by a Proportional Chamber and a Faraday Cup respectively.

In the second experiment, the incident radiation to study the diffraction of real photons was an X-ray beam produced by an Oxford apogee 5000 X-ray tube with a tungsten anode. The high voltage and current were set to 25 keV and 0.300 mA respectively. The X-ray beam was formed by a 2 mm diameter and 0.5 cm thick Pb collimator installed in the input flange. The X-ray beam transverse profile at the target position had an 8 mm radius while the divergence was 4° in both the vertical and horizontal axes.

The observation angle has been set to $150°$, because for this geometry the sources of the initial radiation can be installed in the same flange. Also, because it is close to the backward geometry for which the PXR peaks are more intense and their FWHM is smaller [10, 11].

A tungsten powder constituted of grains which have an average size between $0.8\,\mu m$ and $1.7\,\mu m$ has been chosen as target for three reasons. It has been demonstrated that in such target PXR can be exactly described by the existing theories [10–12]. The contribution of the diffraction of real photons when the electron beam interact with the target has been demonstrated to be negligible [9]. Finally, the diffracted peaks from tungsten are presented in a region free from background peaks between $2.03\,keV$ and $7.39\,keV$.

The powder was sifted in a rectangular cavity $20\,mm \times 9\,mm$ made in $1\,mm$ thick PMMA (methyl methacrylate) supporter. Both sides of the cavity were closed by a $20\,\mu m$ thick mylar foil (biaxially-oriented polyethylene terephthalate BoPET).

The incident radiation interacts with the target, which is mounted in a motorized goniometer with three degrees of freedom. The Diffracted X-rays were registered by a silicon drift detector Amptek X-123 FAST SDD. The effective area of detection is determined by the diameter $4.65\,mm$. All experiments were performed in vacuum with a pressure smaller than 10^{-6} Torr.

3 Results and discussion

The results of both experiments are presented in figure 2. The intensity has been normalized for the Characteristic X-ray Radiation L_l line. It can be observed that the XRD peaks are more intense, have a better peak to background ratio and the measurements show that the FWHM is smaller. Additionally, more XRD peaks are detected, in the case of XRD the (321) peak is clearly visible though it is absent in the PXR spectrum.
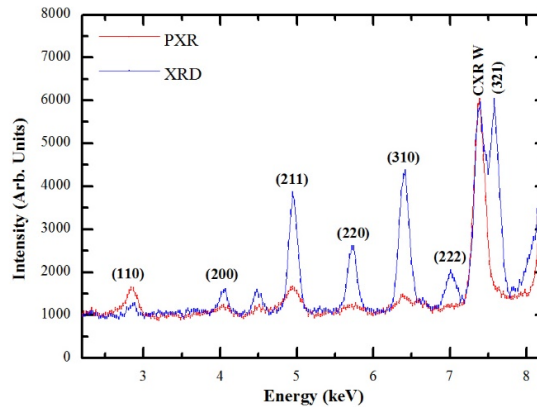
Figure 2. Measured spectra of XRD and PXR normalized according to the intensity of the CXR W L_l line. The statistical error is shown.

In order to obtain a meaningful comparison, the XRD and PXR measurements should be normalized to exclude the influence of three key parameters. The background, the absorption in the target and the spectrum of the incident radiation are substantially different in both processes and their influence should be minimized.

The background has been easily excluded subtracting it from both PXR and XRD spectra. The absorption in the target is considered to be different since during XRD process, real photons enter the material, are diffracted according to Bragg's law and finally exit the target. The radiation is attenuated in the path the photons propagate inside the target $l_{\text{att XRD}}$. On the other hand, during the PXR process, the Coulomb field of the incident particles excite the target electrons, which vibrate emitting photons inside the periodical structure. Finally, these photons exit the target being absorbed only at the exit $l_{\text{att PXR}}$. These considerations have been illustrated in figure 1.

To exclude the influence of attenuation in the target, the spectra without background have been divided by the following attenuation parameters:

$$\left(1 - \exp\left(-\frac{l \sec[\xi - \beta]}{l_{\text{att}}}\right)\right) l_{\text{att}} \cos[\xi - \beta] \sec[\beta] \text{ for PXR}$$

$$\left(1 - \exp\left(-\frac{l (\sec[\xi - \beta] + \sec[\beta])}{l_{\text{att}}}\right)\right) l_{\text{att}} \cos[\xi - \beta](\cos[\xi - \beta] + \cos[\beta])^{-1} \text{ for XRD}$$

For the experimental conditions, $\xi = 30°$, $\beta = 0°$, $l = 1000\,\mu\text{m}$, l_{att} — the attenuation length has been calculated for each energy according to [13].

Finally, PXR and XRD spectra without background and attenuation influence have been divided by the incident radiation spectra. In the case of XRD, the initial spectrum was measured directly from the X-ray tube installing the X-ray detector in the target position. A tungsten collimator 1 mm thick with a 25 μm aperture has been used to limit the intensity. The measured spectrum is presented in figure 3.

On the other hand, the spectrum of equivalent photons constituting the Coulomb field of an electron moving in substance can be obtained by the angle integration of the corresponding spectral-angular distribution [14]:

$$\frac{d^2 N}{d\omega d\theta} = \frac{\alpha}{\pi^2 \omega} \frac{\theta^2}{\left(\theta^2 + \omega_p^2/\omega^2 + \gamma^{-2}\right)^2}$$

where N is the number of photons, α is the fine-structure constant, θ is the angle between the electron velocity and a photon wave-vector, ω_p is the plasma frequency. In the present case ($\omega \ll m$, where m is the electron mass) the upper limit θ_0 of integration with respect to θ should be chosen as $\theta_0 \sim 1$. It is different from the case $\omega \gg m$ considered, for instance, in [15], where $\theta_0 \sim m/\omega$ is chosen (in this case, such choice would lead to $\theta_0 \gg m/\omega$ being unphysical). The obtained result is:

$$\frac{dN}{d\omega} = \frac{2\alpha}{\pi\omega} ln \frac{1}{\sqrt{\omega_p^2/\omega^2 + \gamma^{-2}}}$$

which at sufficiently low energies ($\gamma \ll \omega_p^2/\omega^2$) turns to $\frac{dN}{d\omega} = \frac{2\alpha}{\pi\omega} \ln \gamma$ as shown in figure 3.

Note that the presented expressions for $dN/d\omega$ define the number of virtual photons with logarithmic accuracy. It is associated with the fact that the discussed method of virtual photons is not applicable at very small distances ρ from the particle trajectory and some lower restriction $ρ_0$ (which is not exactly defined) should be imposed upon the impact parameters for the particle interaction with atoms. The presented expressions correspond to the case when the photon flux is integrated with respect to ρ satisfying the relation $ρ > ρ_0$ with $ρ_0 \sim 1/\omega$. For the values of $\hbar\omega$
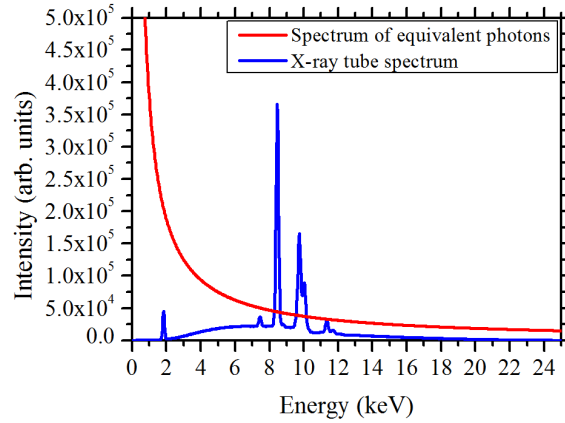
Figure 3. Spectra of the incident radiation. The influence of this parameter has been excluded from the results.

around several kev, $\rho_0 \sim 10^{-8}$ cm, which corresponds to the typical interatomic distance in crystals. It is a rather natural restriction for the distances at which the macroscopic treatment of the medium (involving such quantities as, e. g., ω_p in this case) is valid. The expressions for the virtual photon flux spectral density for arbitrary ρ_0, as well as the tips for choosing the proper value of ρ_0 in various cases, can be found in [16].

The spectra without the influence of background, attenuation in the target and incident radiation spectrum are shown in figure 4. The spectra have been normalized to the intensity of the (310) peak to achieve a better visualization.
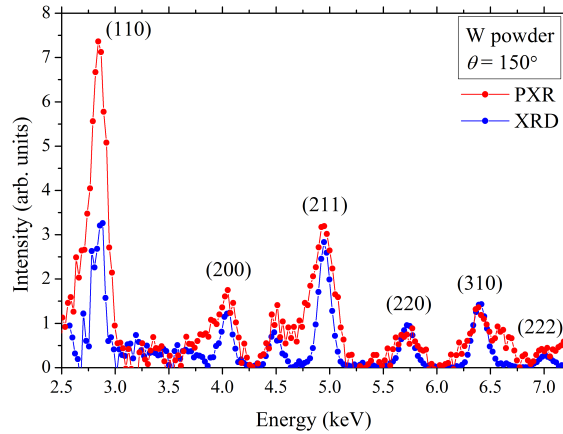
Figure 4. Spectra of XRD and PXR normalized according to the intensity of the (310) diffracted peak. The influence of the background, incidence radiation spectrum and attenuation in the target has been excluded.

It can be observed that for the presented normalization the intensity of the PXR signal is bigger than the intensity of the XRD signal for the lower energy diffracted peaks. However, this tendency changes when the diffracted peak energy increases. Since the key parameters that determine the differences in the diffraction processes have been excluded, one could expect the diffracted spectra to be similar, nevertheless a clear difference exits.

In order to highlight this behaviour, the integral of each PXR diffraction peak was divided by the corresponding integral of each XRD diffraction peak. Far from being similar, it can be clearly observed that the ratio decreases when the energy increases as shown in figure 5. The results evidences that some factors that influence in the diffraction processes have been omitted.
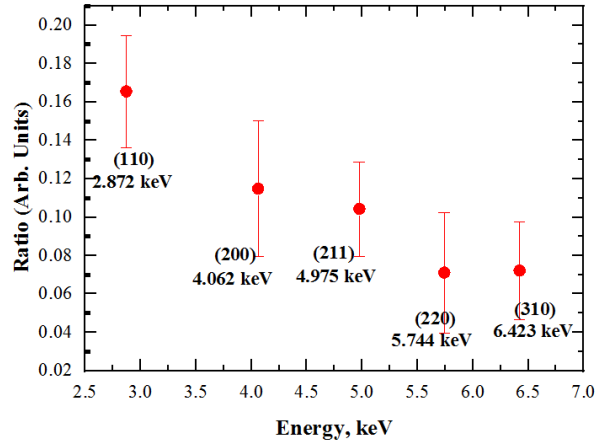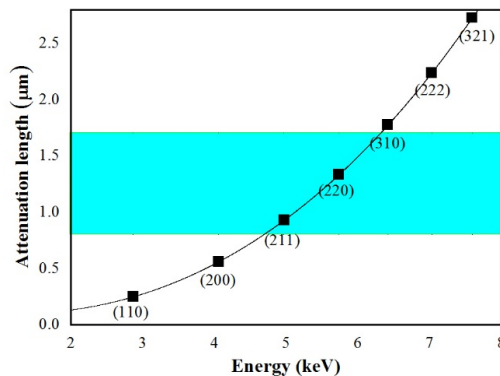

Figure 5. The ratio between the integral number of counts of PXR by XRD diffracted peaks.

The influence of the formation length in the behaviour described in figure 5 can be excluded or at least minimized, since it has been mentioned that the formation length for PXR is proportional to the attenuation length [12]. In the performed experiment, the crystallites dimensions are larger than the attenuation length for the peaks (110) and (200) as shown in figure 6. It is the ratio for these peaks that decreases more sharply in figure 5.

Additionally, the absolute comparison of PXR from powders with theory showed a good agreement which means that the diffraction occurs at saturation for this target [11]. The influence of the formation length could be reflected in the absence of the (321) peak, since the crystallite dimensions are smaller than the attenuation length for that peak.

Anyway, the formation length for PXR is a variable that should be analysed further.

Figure 6. Attenuation length in tungsten according to the photon energy. The energy for diffracted peaks at $\theta = 150°$ is shown by squares. The crystallite dimensions of the target are shown in the underlined region.

4 Conclusions

The ratio between the integral number of counts of PXR and XRD diffracted peaks decreases when the peak energy increases. The influence of the formation length of PXR cannot be used to explain the behaviour.

It is possible to suppose that the absence of the (321) PXR peak is a direct consequence of the PXR peak intensity decrease when the energy increases. This effect could be related to the crystallite dimensions, which are smaller than the formation length for the PXR peak.

The differences in the diffraction processes of real and virtual photons cannot be explained only based on the background, the absorption in the target and the spectrum of the incident radiation.

Acknowledgments

References

[1] M.L. Ter-Mikaelian, *High Energy Electromagnetic Processes in Condensed Media*, John Wiley & Sons, New York, NY, U.S.A. (1972).

[2] V. Baryshevsky and I. Feranchuk, *Parametric X-rays from ultrarelativistic electrons in a crystal : theory and possibilities of practical utilization*, *J. Phys. France* **44** (1983) 913.

[3] S.A. Vorob'ev, B.N. Kalinin, S. Pak and A.P. Potylitsyn, *Detection of monochromatic X-ray emission in the interaction of ultrarelativistic electrons with a diamond single crystal*, *J. Exp. Theor. Phys. Lett.* **41** (1985) 1.

[4] A.P. Potylitsyn, *Parametric X-ray Radiation*, in *Electromagnetic Radiation of Electrons in Periodic Structures*, Springer Berlin Heidelberg, Berlin, Heidelberg (2011), pp. 105–133.

[5] E.J. Williams, *Correlation of certain collision problems with radiation theory*, *Kong. Dan. Vid. Sel. Mat. Fys. Med.* **13** (1935) 1.

[6] C.F. Weizsäcker, *Ausstrahlung bei Stößen sehr schneller Elektronen*, *Zeit. Phys.* **88** (1934) 612.

[7] E. Fermi, *Über die Theorie des Stoßes zwischen Atomen und elektrisch geladenen Teilchen*, *Zeit. Phys.* **29** (1924) 315.

[8] V.G. Baryshevsky, I.D. Feranchuk and A.P. Ulyanenkov, *Electromagnetic Radiation from a Charged Particle in Crystals: Qualitative Consideration*, in *Parametric X-Ray Radiation in Crystals: Theory, Experiment and Applications*, Springer Berlin Heidelberg, Berlin, Heidelberg (2005), pp. 1–17.

[9] V.I. Alexeyev, A.N. Eliseyev, E. Irribarra, I.A. Kishin, A.S. Kubankin and R.M. Nazhmudinov, *Observation of parametric X-ray radiation in an anomalous diffraction region*, *Phys. Lett.* **A 380** (2016) 2892.

[10] V. Astapenko, N. Nasonov and P. Zhukova, *Anomalous peak in the spectrum of polarizational bremsstrahlung from relativistic electrons moving through a solid target*, *J. Phys.* **B 40** (2007) 1337.

[11] V. Alekseev, A. Eliseyev, E. Irribarra, I. Kishin, A. Klyuev, A. Kubankin et al., *Parametric X-ray radiation from powders*, *Phys. Lett.* **A 383** (2019) 770.

[12] N. Nasonov, *Collective effects in the polarization bremsstrahlung of relativistic electrons in condensed media*, *Nucle. Instrum. Meth.* **B 145** (1998) 19.

[13] B. Henke, E. Gullikson and J. Davis, *X-ray interactions: Photoabsorption, scattering, transmission, and reflection at E = 50–30,000 eV, Z = 1–92*, *Atom. Data Nucl. Data* **54** (1993) 181.

[14] X. Artru and P. Rullhusen, *Parametric x-rays and diffracted transition radiation in perfect and mosaic crystals*, *Nucl. Instrum. Meth.* **B 145** (1998) 1.

[15] V. Berestetskii, E. Lifshitz and L. Pitaevskii, *Radiative Corrections*, in *Quantum Electrodynamics*, Elsevier (1982), pp. 501–596.

[16] J.D. Jackson, *Classical Electrodynamics*, Third edition, John Wiley & Sons, Inc. (1999).